**Atmospheric
Chemistry
and Physics**
Discussions

Open Access

Sensitivity of tropospheric loads and lifetimes of short lived pollutants to fire emissions

N. Daskalakis[1,2], S. Myriokefalitakis[1], and M. Kanakidou[1]

[1]Environmental Chemical Processes Laboratory, Department of Chemistry, University of Crete, Heraklion, Crete, Greece
[2]Institute of Chemical Engineering Sciences (ICE-HT), Forth, Patra, Greece

---

ACPD

14, 22639–22676, 2014

Sensitivity of tropospheric loads and lifetimes of short lived pollutants

N. Daskalakis et al.

Title Page

Abstract	Introduction
Conclusions	References
Tables	Figures

|◄ | ►|
◄ | ►

Back | Close

Full Screen / Esc

Printer-friendly Version

Interactive Discussion

Abstract

The capability of global Chemistry and Transport Models (CTMs) to simulate atmospheric composition and its spatial and temporal changes highly relies on the input data used by the models, in particular the emission inventories. Biomass burning emissions show large spatial, daily, seasonal and year-to-year variability. In the present study, we applied a global 3-D CTM to evaluate uncertainties in the computed atmospheric composition associated with the use of different biomass burning emissions and identify areas where observational data can improve in reducing these uncertainties. We find the emission inventory choice to be able to introduce regional differences in the calculated load of aerosols up to a factor of 4. Assumptions on the injection height of the biomass burning emissions are found to produce regionally up to 30 % differences in the calculated tropospheric lifetimes of pollutants. Computed changes in lifetimes point to a strong chemical feedback mechanism between emissions from biomass burning and isoprene emissions from vegetation that are linked via oxidant chemistry. These interactions reduce isoprene load in the presence of biomass burning emissions by 15 %, calculated for the same amount of isoprene emitted into the troposphere. Thus, isoprene load and lifetime are inversely related to the quantities of pollutants emitted by biomass burning. This feedback is shown to be able to increase the effective secondary aerosol yield from isoprene by up to 40 %.

1 Introduction

Atmospheric composition is affected by emissions of reactive gases and aerosols to the atmosphere by several natural (e.g. soils, vegetation, oceans, volcanoes, wild fires) and anthropogenic sources (e.g. industrial and residential activities, transport, and shipping). Among these sources biomass burning plays a central role for atmospheric chemistry via changes in the atmospheric composition but also impacting on the ecosystem functioning through atmospheric deposition of nutrients and the lifecy-

cle of vegetation (Keywood et al., 2013). Biomass burning is positioned between the natural (wild fires) and human-induced (intentional burning) sources of atmospheric pollutants since a fraction of open fires is induced by humans for agricultural and city expansion purposes (Levine et al., 1995) or for protection against fire itself (Mutch,
5   1994). Biomass burning is important source of trace constituents to the atmosphere including radiatively and chemically reactive gases and aerosols (Akagi et al., 2011; Andreae and Merlet, 2001). It is the largest source of primary carbonaceous aerosols (Bond et al., 2004) and the second largest source of volatile organic compounds (VOC) in the atmosphere after the emissions from vegetation (Guenther et al., 2012) and of
10 carbon monoxide (CO) after anthropogenic emissions (Kanakidou and Crutzen, 1999; Pfister et al., 2005).

Emissions from biomass burning and their transformation in the atmosphere affect air quality (Lelieveld et al., 2004), interact with radiation (Reid et al., 2005) and the atmospheric water cycle and thus affect climate (Rosenfeld, 1999). In turn climate change
15 is seen to impact on wild fire occurrence and intensity. For instance the exceptionally intensive 1997/98 Indonesia fires have been attributed to the combined strength of the El Niño and the Indian Ocean Dipole (Field et al., 2009).

Significant observed changes in the trends of atmospheric concentrations of CH_4 and CO have been attributed to the changes in the biomass burning emissions (Sim-
20 monds et al., 2005). Most of these emissions occur in the tropics that are subject to intensive photochemistry in the presence of high humidity conditions and significant convective activities (Chatfield and Delany, 1990; Crutzen, 1994). During summer in the high latitudes, boreal forest fires contribute about 12 % to the global biomass burning (Lavoué et al., 2000) and can be so intensive and convective to reach the high
25 troposphere and low stratosphere (Fromm et al., 2000). Tropical photochemistry is controlling the lifetime of most atmospheric pollutants (Crutzen, 1994), including reactive greenhouse gases like methane (CH_4) and ozone (O_3), and thus their persistence in the atmosphere to impact on radiation and climate. Up to about 25 % of the net global photochemical production of tropospheric ozone has been attributed to biomass burn-

N. Daskalakis et al.

ing emissions and chemistry in the atmosphere (Crutzen and Andreae, 1990). Long range transport of biomass burning aerosols has been seen to happen fast within one or two weeks both downwind tropical (Dirksen et al., 2009; Edwards et al., 2006) and high latitude sources (Jaffe et al., 2004). Thus this source is affecting atmospheric pollutants levels in remote environments. For instance, chemical ageing of fire plumes has been identified as contributor to the high ozone over the Atlantic ocean (Lelieveld et al., 2004). Therefore it is important to simulate the impact of biomass burning emissions on tropospheric composition and pollutant lifetimes and to evaluate the uncertainties in such simulations.

Several biomass burning emission inventories have been constructed based on satellite observations (van der Werf et al., 2010), experimentally determined pollutant emission factors (Andreae and Merlet, 2001) and assumptions on the state of burning of the biomass (smoldering or flaming, van der Werf et al., 2006). All these factors introduce uncertainties in the emissions (Granier et al., 2011). The injection height of the fire emissions (Dentener et al., 2006; Sofiev et al., 2012) is an additional cause of discrepancies in the model estimates of the impact of these fires on tropospheric composition. The height distribution proposed by Dentener et al. (2006) (used in this work) is based on wildfire location and type, where the distribution described in Sofiev et al. (2012) is based on the fire characteristics (fire intensity, temperature of plume, type of source) as well as the meteorological conditions (atmospheric boundary layer height, free troposphere). These two approaches show similarities in emission heights over North America and Oceania, where over Eurasia, Australia and South America the two methods show significant differences (Sofiev et al., 2013). Plume height climatology over North America has been also derived by analysis of 5 year satellite observations by MISR (Val Martin et al., 2010). Plume rise models evaluated against that climatology have been shown to underestimate the observed plume heights (Val Martin et al., 2012). Guan et al. (2008) using the NCAR CAM3.1 model found that the calculated CO concentrations downwind biomass burning emission areas, can increase by up to 150 ppb depending on the assumptions in the injection height of the

emissions. Boreal forest fire emissions occurring high in the troposphere have been detected by Colarco et al. (2004) to be transported from Canada to Washington DC in the USA where they have been mixed with boundary layer air. The long range transport of biomass burning pollutants has been followed by lidar and satellite observations and the simulations have been shown to be sensitive to the injection height of the emissions as well as to the entrainment of air into the boundary layer over USA. Note that boreal fires plumes can reach the upper troposphere where their impact is different from that in the boundary layer due to the non-linearity in chemistry (Chatfield and Delany, 1990) and the different photochemical conditions there. Leung et al. (2007) global modeling study of the impact of boreal fire emissions on air pollutants levels, found a much larger enhancement in ozone when about half the emissions are released above the boundary layer than all emissions are occurring in the boundary layer. They attributed these differences to the role of peroxyacetyl nitrate (PAN) as carrier of NO_x downwind burning areas. Jaffe et al. (2004) found that the intensive Siberian fires in 2003 enhanced the background ozone over the Pacific Norhwest, resulting to exceedance of ozone air quality standard. Hodzic et al. (2006) studying AOT over Europe during the 2003 Portuguese fires identified high altitude transport of smoke particles from Portugal to the Netherlands, that has been both observed by POLDER-2 and simulated by the CHIMERE model. Williams et al. (2012) simulated the African fires in 2005 using the TM4 model and three different biomass burning emission inventories, two global and one regional. They calculated differences in the ozone global burden resulting from the use of different biomass burning inventories that range between +1.7 % and +4.6 %.

In the present study we applied a global 3-D Chemistry and Transport Model (CTM) to evaluate uncertainties in the computed atmospheric composition and major pollutants lifetimes associated with the use of different recently updated and commonly used biomass burning emissions. We also identify areas where observational data can improve in reducing these uncertainties.

Title Page

Abstract	Introduction
Conclusions	References
Tables	Figures

|◄ | ►|
| ◄ | ► |

| Back | Close |

Full Screen / Esc

Printer-friendly Version

Interactive Discussion

2 Model description

The model used for this study is the global 3-D CTM TM4-ECPL (Kanakidou et al., 2012). The model accounts for gas and multiphase chemistry to describe tropospheric ozone chemistry and all major aerosol components (primary and secondary). It con-

5 tains explicit chemistry of C_1 to C_5 volatile organic compounds (VOCs) and a highly simplified α-pinene and β-pinene chemistry. The model calculates secondary organic aerosol (SOA) formation by VOC oxidation and subsequent gas-to-particle partitioning of semivolatile products (Tsigaridis and Kanakidou, 2007, as updated by Myriokefali-takis et al., 2010). Chemical ageing of organic aerosol (OA) is also taken into account.

10 For primary organic aerosol (POA) chemical ageing is driven by O_3 and for SOA by OH (Tsigaridis and Kanakidou, 2003). Multiphase chemical production of SOA is parame-terized as described in Myriokefalitakis et al. (2011). Gas-to-particle partitioning of in-organic components is solved using the ISORROPIA II aerosol thermodynamic model that also calculates the aerosol-water (Fountoukis and Nenes, 2007; Nenes et al.,

15 1998). For this study the TM4-ECPL model uses a $3° \times 2°$ longitude–latitude grid and 34 hybrid levels up to 0.1 hPa and is driven by the European Centre for Medium-range Weather Forecasts (ECMWF) ERA-Interim meteorological data (Dee et al., 2011) for all the sensitivity simulations.

2.1 Natural emissions

20 Isoprene, terpenes and biogenic volatile organic compounds (BVOC) emissions in the TM4-ECPL model are taken from the MEGANv2 inventory (Guenther et al., 2012) made available at the ECCAD (Emissions of atmospheric Compounds and Compila-tion of Ancillary Data) website (http://eccad.sedoo.fr) for the year 2000. This inventory has been then scaled for the year 2008 based on global emission estimates provided

25 by the PEGASOS (Pan European Gas-AeroSOls-climate interaction Study) project. Dust emissions are from AeroCom (Aerosol Comparisons between Observations and Models; Dentener et al., 2006) calculated for the year 2008 by E. Vignati (personal

communication, 2011). Marine emissions of sea-salt aerosols and organic gases and aerosols are calculated online driven by meteorology and sea water productivity as described by Myriokefalitakis et al. (2010) and Vignati et al. (2010).

2.2 Anthropogenic emissions

Anthropogenic emissions used for this experiment are the ECLIPSE (Evaluating the CLimate and Air Quality ImPacts of Short-livEd Pollutants) version 4.0 emissions (Klimont et al., 2013), available in 0.5° × 0.5° spatial resolution. The ECLIPSE anthropogenic inventory was initially provided as sectoral including the agricultural waste burning sector (AWB). Since AWB is either considered to be anthropogenic or part of the biomass burning emissions, caution was taken to avoid double counting of the emissions. For this, whenever AWB was included in the biomass burning emission inventory (FINN, GFEDv3, see Sect. 2.3 for more information) used in this study, it was removed from the anthropogenic emissions, since the study is biomass burning-centered. The AWB amounts to 26.7 % of the total pollutants emissions (approximately $34.5\,\mathrm{Tg\,a^{-1}}$) for the year 2008 (see Table 1 for more information). Anthropogenic emissions of all basic pollutants are used (CO, nitrogen oxides (NO_x), black carbon aerosol (BC), particulate organic carbon (OC), sulfur dioxide and sulfates (SO_x) as well as speciated non methane volatile organic compounds (NMVOCs; for a list of the NMVOCs used in the model see Supplement S1).

2.3 Biomass burning emissions

For the present study a number of sensitivity simulations have been performed using different biomass burning emissions (Table 2). For the base simulation (S0.0), the Global Fire Emission Database v 3.1 (GFEDv3; van der Werf et al., 2010) is used, excluding the AWB sector (Table 3), hereafter called GFEDv3-ECLIPSE biomass burning emissions (S0.X), since this has been performed in the framework of the ECLIPSE project. Additional simulations (Table 4) using the original GFEDv3 (van der Werf et al.,

2010) (S1.X), the Atmospheric Chemistry and Climate Model Intercomparison Project's (ACCMIP; Lamarque et al., 2013) biomass burning emissions (S2.X), the Fire INventory from NCAR (FINN; Wiedinmyer et al., 2011) (S3.X) and a simulation where no biomass burning emissions were taken into account (S4.0) have been performed. Since the injection height of these emissions contributes to the uncertainty of the model results, biomass burning emissions are considered in the model either to be injected at heights following Dentener et al. (2006), or to be emitted solely at the surface (see list of simulations in Table 4). The temporal variability of theses biomass burning inventories per emitted species for 2008 is shown in Fig. 1. This figure depicts the differences between the inventories in their seasonality and amplitude (also annual totals in Table 2). The FINN inventory shows the largest magnitude in the temporal variation of these emissions. On the opposite, ACCMIP shows the smallest seasonality, in particular for OC, BC and NH_3. The differences between GFEDv3-ECLIPSE and GFEDv3 provide information on the seasonality and amounts of the AWB emissions as calculated and provided by the GFEDv3 database. The AWB emissions that have been excluded from the GFEDv3-ECLIPSE biomass burning inventory significantly contribute to NMVOC and NH_3 emissions during spring and summer.

3 Experiment setup

The impact of the use of different biomass burning emission inventories to the calculated tropospheric loads and lifetimes of the main pollutants and the robustness of model results with regard to the wild fire emissions have been evaluated based on nine different simulations. For all simulations the model setup was exactly the same, except for the biomass burning emissions inventory used and its vertical distribution application. A summary of the simulations here performed is provided in Table 4. The GFEDv3-ECLIPSE inventory and height distribution for biomass burning emissions have been used as the base case scenario (S0.0). All scenarios named SX.0 assume the same fractional height distribution of the emissions according to Dentener et al. (2006) where

Title Page

Abstract · Introduction

Conclusions · References

Tables · Figures

|◄ · ►|

◄ · ►

Back · Close

Full Screen / Esc

Printer-friendly Version

Interactive Discussion

all the scenarios named SX.1 assume all open biomass burning emissions to occur at surface. For scenario S4.0, open biomass burning emissions are set to zero.

4 Results

To evaluate the ability of the model to reproduce the observations, the computed concentrations are compared with measurements. The differences in the fields computed by the various emission inventories provide a measure for the robustness of the model results with regard to the biomass burning impacts. Comparison of the simulated tropospheric concentrations of pollutants between the various scenarios reveals the spatial and temporal differences due to the different inventories. These differences can point to areas where additional observations can contribute to reduce uncertainties of the emission inventories. Finally, tropospheric lifetimes are calculated to provide information on how the location and strength of the emissions affect the persistence of the pollutants in the atmosphere.

4.1 Comparison with ground measurements

Surface observations of Ozone from the European Monitoring and Evaluation Programme (EMEP) monitoring network (Europe), Ozone and CO observations from the World Data Centre for Greenhouse Gases (WDCGG) database (Global) and particulate Organic Carbon (OC) observations from the Aerosol Comparisons between Observations and Models (AeroCom) phase II database (Global) (Tsigaridis et al., 2014) have been used for the model evaluation. The locations of measurements are shown in Fig. S1 in the Supplement. Characteristic comparisons at selected stations are shown for OC (Fig. 2), CO (Fig. 3) and O_3 (Fig. 4). Primary pollutants emitted by biomass burning are the mostly affected ones by the different emission inventories and injection heights. Thus, OC computed concentrations (Fig. 2) and BC concentrations (not

shown) present the largest diversity, between simulations followed by CO (Fig. 3), which is emitted by fires, but has also secondary sources.

The simulated OC for the various scenarios and their differences from the observations in the tropics, the subtropics and high latitudes at locations affected by biomass
5 burning emissions are shown in Fig. 2. Due to limited observational data from the tropics where most of the biomass burning occurs, for the following comparisons all available data have been used independent of the year. Modeled differences for OC due to emission inventory choice can exceed a factor of three at Alta Floresta (Fig. 2c) and eight at Rondonia (Fig. 2d) during the biomass burning months. Using the ACCMIP in-
10 ventory the largest OC levels are computed at the tropical station of Alta Floresta in August and September, whereas the GFEDv3-ECLIPSE and GFEDv3 inventories include large amounts of OC injections at the subtropical stations of California in June, July and August (Fig. 2b and g). Different emission inventories significantly affect the model performance over and downwind locations where wildfires occur. The use of GFEDv3
15 and ACCMIP inventories in CTMs has been discussed by Tsigaridis et al. (2014).

Similar results are obtained for CO, as seen in Fig. 3, where during the biomass burning season different quantities of CO are calculated depending on the inventory used. At Yonagunijima (Fig. 3a) CO concentration differences computed using the different inventories maximize in spring and models are underestimating measurements
20 by 25 %. Such differences between inventories are large at the East Trout Lake station in Canada, where in June and July model results differ by up to 150 ppb (a factor of 2.5). These results reflect the extremely high emissions in the GFEDv3-ECLIPSE and GFEDv3 inventories for this region that are not seen in the measurements (Fig. 3b). The assumption that all emissions occur near the surface leads to about 60 % higher
25 CO surface concentrations than when emissions are distributed vertically. At the areas where biomass burning occurs and downwind of them, these emissions contribute between 10 and 75 % to the total CO levels during the burning season.

Comparisons of O_3 simulations with measurements (Fig. 4) show noticeable difference between the simulation that neglects wildfire emissions (S4.0) and all other sim-

ulations, at stations like Mt. Kenya (Fig. 4f), La Quiaca observatory (Fig. 4g) and Hok Tsui (Fig. 4d), which are located in the vicinity or outflow of tropical biomass burning. These are areas where O_3 levels are the most sensitive to the different biomass burning emission scenarios. For instance, at La Quiana observatory (Fig. 4g), differences as high as 10 ppb of O_3 (i.e. ~ 25 %) are computed for October when using the different emission scenarios. The FINN inventory results in the highest computed O_3 levels, while omitting biomass burning reduces O_3 levels by ~ 35 %. However, very small sensitivity is seen between the scenarios with wildfire emissions for the other locations in Fig. 4. Thus, evaluating these inventories requires air quality monitoring close to the major biomass burning sources in the tropics, which are virtually absent.

4.2 Tropospheric loads

The global annual mean tropospheric loads for selected gases and aerosol components as computed for the base case scenario (S0.0) are shown in Fig. 5 for OC, CO, NO_x, O_3, OH, and isoprene. Figure S2 (in the Supplement) shows similar results for BC, SO_4^{2-}, NO_3^-, HNO_3 and NH_4^+. Although changes in the wildfire emissions do not significantly impact the global tropospheric load of most pollutants as shown in Table 5, regionally significant differences are computed (e.g. for BC, the difference can reach a factor of 7, Fig. S3b) as will be further discussed. The choice of wildfire emission inventory impacts on the calculated tropospheric load of tracers. The most sensitive pollutants to wildfire emissions are found to be OC and BC, while O_3 shows small sensitivity.

4.2.1 Contribution of wildfires emissions on tropospheric loads

The contribution of wildfires to the tropospheric load of pollutants can be calculated by comparison of S0.0 (base case) with S4.0 that neglects the emissions. Wildfires increase the tropospheric loads of: OC by ~ 30 %, BC by ~ 35 %, CO by about 13 %, NH_4^+ by 10 %, HNO_3 by 8 %, NO_x by 5 %, and SO_4^{2-} and O_3 by 3 % (Table 5). Pre-

vious studies for CO with the NOAA GFDL GCTM have shown biomass burning to contribute from 15 to 30 % to the total CO background (Galanter et al., 2000). This impact presents large temporal and spatial variability since it occurs during the burning season that lasts only a few months per year and is marked by tropical and boreal forest fires. Also O_3 load has been shown to correlate with CO load during biomass burning events with a slope of O_3/CO of about 1 (Honrath et al., 2004). The spatial variability of the annual mean impact of wildfire emissions on the tropospheric loads of OC, CO, NO_x, O_3, OH and isoprene is depicted in Fig. 6a–f and on BC, SO_4^{2-}, NO_3^-, HNO_3 and NH_4^+ in Fig. S4a–e (Supplement). The most affected pollutants are OC (Fig. 6a) and BC (Fig. S4a) with local reduction due to the omission of wildfires by almost 100 %, while annual mean local impacts on O_3 and CO, pollutants that have strong secondary sources, maximize at 20–30 % in the tropics. As expected, the NO_x tropospheric load is mostly affected by biomass burning in the extra-tropics at the outflow of boreal fires and over the tropical regions of south America, Africa and N. Australia where burning is significant (Fig. 6c). As a consequence of the NO_x and O_3 reductions when fire emissions are omitted, the computed hydroxyl radical (OH) load (Fig. 6e) is significantly reduced (5–10 %) over the same regions.

4.2.2 Impact of injection height

The effect of height distribution of wildfire emissions on the computed tropospheric loads has been studied by comparing the simulations SX.0 with the respective simulations SX.1. Figure 7 presents such comparisons for OC and BC. Both OC and BC are strongly affected by the injection height parameterization, since emitting aerosols above the surface (and even more, above the boundary layer) reduces aerosols available near the surface for loss via dry deposition. The largest differences are computed for the high latitudes over N. America and China where emission height distribution assumptions can result to about 25 % differences (Fig. 7a). Previous studies conducted with GEOS-Chem model over the south eastern Asia during 2001, show a decrease of 20–40 % of BC surface concentrations when injected at height (Jian and Fu, 2014).

In the same study it is shown that biomass burning injection height has much larger impact on BC than CO (50–150 % more BC calculated at 700 hPa, than when emitted in the boundary layer). Differences are positive over source areas (since more is emitted near the surface in SX.1) and negative downwind (since less is transported away from source regions due to the increased deposition flux at the source regions). Additional comparisons are presented in the Supplement (Fig. S5a–f). Assumptions in the biomass burning emissions injection height marginally affect CO and O_3, with computed differences in the global annual mean tropospheric load smaller than 2.5 %.

4.2.3 Chemical feedbacks between biomass burning and vegetation emissions

It is interesting to examine the impact of wildfire emissions on isoprene tropospheric load. Isoprene is the single most important biogenic volatile organic compound (BVOC) emitted by vegetation (more than 50 % of total annual BVOC emissions). The changes in OH described in Sect. 4.2.1 (Fig. 6e), the main tropospheric oxidant that consumes isoprene, led to opposite in sign changes of isoprene (Fig. 6f). Such results indicate a strong chemical feedback between biomass burning and vegetation emitted species that occurs via their impact on oxidant chemistry. This feedback increases by about 40 % the mean effective aerosol yield from isoprene that is derived as the ratio of the tropospheric load of isoprene-SOA to that of isoprene. Impacts on the effective yields of the first generation gaseous products of isoprene are smaller of the order of 7–8 %.

When biomass burning does not occur, up to 10 % more isoprene is calculated locally for the same amount of isoprene emissions (S4.0) due to lower oxidants and thus reduction in isoprene's chemical losses. These results demonstrate the strong coupling between tropospheric chemistry, biomass burning and vegetation emitted species. They show that it is critical for the evaluation of the impact of these emissions on tropospheric chemistry to consistently account for BVOC emissions from vegetation and the co-location/co-occurrence of biomass burning emissions in the area.

4.3 Tropospheric lifetimes

Changes in chemistry as discussed above, as well as changes in deposition of pollutants due to the modification of their spatial distribution, affect the lifetime of these compounds in the troposphere. Thus, isoprene's lifetime is increased in S4.0, as previously explained, by almost 20 % compared to S0.0. The global tropospheric lifetimes of all other species are less impacted by the choice of the emission inventory, with a maximum of about 12 % for OC. This is in agreement with previously calculated differences reported in literature. For instance, such differences resulting from the use of 3 different biomass burning inventories (two global and one regional) in the TM4 model coupled with the CBM4 chemical mechanism do not exceed 5 % for the African domain (Williams et al., 2012). Table 6 shows the calculated global tropospheric lifetimes of pollutants for each scenario. The maximum percentage differences from the base case scenario (S0.0) are computed for the S4.0 simulation that neglects all wildfire emissions.

The lifetimes of pollutants, computed as the ratio of the tropospheric load to the loss rate (sum of chemical loss and deposition fluxes) for each model grid, show sensitivity to both the height distribution of the emissions and the different emission inventories. The sensitivity of the OC and BC lifetime to the height of injection of the biomass burning emissions is depicted in Fig. 8, where the difference in calculated tropospheric lifetimes of OC attributed to emission injection height alone can reach 30 % (right panels). The differences produced by injection height for more species are provided in Fig. S6 (Supplement). The use of different biomass burning emission inventories led to up to almost 90 % local differences for OC as seen in Fig. 8g. The maximum differences are computed in the tropics and over the boreal forests in Canada and eastern Russia using the ACCMIP and FINN inventories (Fig. 8e and g). The overall impact of biomass burning emissions (simulations S4.0 vs. S0.0) on the regional lifetimes of tracers is shown in Fig. 9, where significant increases in O_3 (up to about 25 %) and CO (up to about a factor of 2) lifetimes are calculated when wild fire emissions are neglected.

Title Page

Abstract | Introduction

Conclusions | References

Tables | Figures

|◄ | ►|

◄ | ►

Back | Close

Full Screen / Esc

Printer-friendly Version

Interactive Discussion

Biomass burning is reducing O_3 lifetime in the burning regions of the tropics and the boreal forests. This is mainly due to the reaction of O_3 with NO emissions and subsequent HNO_3 formation. The impact of fire emissions on chemistry can be seen through the increases in the regional lifetime of CO and isoprene in S4.0 (Fig. 9a and d), where local differences can reach 160 %. OC and BC lifetimes are highly affected with local computed differences up to almost 90 % (OC) and 150 % (BC) (Fig. 9e and f). Similar results are produced for SO_4^{2-} lifetimes where the local differences in calculated tropospheric lifetimes range from about −25 % to 25 % near the tropics (Fig. 9g) and above the boreal forests of Russia and Canada where most open biomass burning events occur.

The tropospheric NO_y lifetime (NO_y = sum of NO_x, HNO_3, peroxyacetyl nitrate and organic nitrates) strongly responds to the wild fire emissions used in the model, with differences between about −40 % and +60 %. When wild fire emissions are omitted in the model, the NO_x lifetime is increased by about 75 % locally (Fig. 10), although on global scale a smaller lifetime change is computed (Table 6). Figure 10 depicts large local differences between the different scenarios even in the sign of lifetime changes. Focusing on central Canada and north eastern Asia, the S2.0 simulation results in a large increase in NO_x lifetime compared to S0.0 that is weaker for the S1.0. These differences are mainly attributed to the spatial distribution of the emissions favoring different chemistry pathways and resulting in different dry and wet removal fluxes.

5 Conclusions

The CTM sensitivity simulations performed here show that the choice of wildfire emission inventory has a significant impact on the simulated tropospheric concentrations of both primary emitted and secondary produced species, and as a result on the tropospheric lifetimes of gaseous and aerosol pollutants. The differences introduced by the choice of biomass burning emissions are usually between −30 and 30 % above and downwind of biomass burning hotspots (near the tropics, boreal forests of Russia and

Canada) and can reach up to a factor of about 7 (e.g. for BC Fig. S3). These impacts maximize for primary pollutants over source areas and for secondary pollutants downwind. Differences are computed either because of spatial and temporal differences in the emitted amounts of primary pollutants, or because of the resulting changes in the levels of oxidants and thus the impact of the primary pollutants to the concentrations of the chemically produced tracers. Thus, isoprene, mainly emitted by vegetation, shows sensitivity to the biomass burning emissions, with increasing tropospheric concentrations (and lifetime) when fire emissions decrease mainly due to the reduction in OH radical concentrations. This results in an increase of the mean effective aerosol yield from isoprene by about 40 % and for the first generation gaseous products by about 7 % when biomass burning emissions are taken into account. Since the meteorology remains the same between the sensitivity simulations, all species are subject to the same wet removal rates both spatially and temporally, regardless of simulation.

The height distribution of the wildfire emissions is found to affect both the tropospheric load and the lifetimes of the pollutants. OC is mostly affected with regional differences attributed only to different emission height distribution ranging from −20 % to 25 % and those attributed to the different emission inventories ranging from −70 % to 450 % (Fig. S7b). Finally observations in the tropics and the high latitudes at locations affected by biomass burning are extremely limited. The observational network at these locations needs to be carefully strengthened to provide invaluable information to improve biomass burning emission inventories.

The Supplement related to this article is available online at doi:10.5194/acpd-14-22639-2014-supplement.

References

Akagi, S. K., Yokelson, R. J., Wiedinmyer, C., Alvarado, M. J., Reid, J. S., Karl, T., Crounse, J. D., and Wennberg, P. O.: Emission factors for open and domestic biomass burning for use in atmospheric models, Atmos. Chem. Phys., 11, 4039–4072, doi:10.5194/acp-11-4039-2011, 2011.

Andreae, M. O. and Merlet, P.: Emission of trace gases and aerosols from biomass burning, Global Biogeochem. Cy., 15, 955–966, 2001.

Bond, T. C., Streets, D. G., Yarber, K. F., Nelson, S. M., Woo, J.-H., and Klimont, Z.: A technology-based global inventory of black and organic carbon emissions from combustion, J. Geophys. Res.-Atmos., 109, D14203, doi:10.1029/2003JD003697, 2004.

Chatfield, R. B. and Delany, A. C.: Convection links biomass burning to increased tropical ozone: however, models will tend to overpredict O_3, J. Geophys. Res.-Atmos., 95, 18473–18488, 1990.

Colarco, P. R., Schoeberl, M. R., Doddridge, B. G., Marufu, L. T., Torres, O., and Welton, E. J.: Transport of smoke from Canadian forest fires to the surface near Washington, D.C.: injection height, entrainment, and optical properties, J. Geophys. Res.-Atmos., 109, D06203, doi:10.1029/2003JD004248, 2004.

Crutzen, P. J.: An overview of atmospheric chemistry, in: Topics in Atmospheric and Interstellar Physics and Chemistry, edited by: Boutron, C. F., Les Editions de Physique, Les Ulis, France, 1994.

Crutzen, P. J. and Andreae, M. O.: Biomass burning in the tropics: impact on atmospheric chemistry and biogeochemical cycles, Science, 250, 1669–1678, 1990.

Dee, D. P., Uppala, S. M., Simmons, A. J., Berrisford, P., Poli, P., Kobayashi, S., Andrae, U., Balmaseda, M. A., Balsamo, G., Bauer, P., Bechtold, P., Beljaars, A. C. M., van de Berg, L., Bidlot, J., Bormann, N., Delsol, C., Dragani, R., Fuentes, M., Geer, A. J., Haimberger, L., Healy, S. B., Hersbach, H., Hólm, E. V., Isaksen, L., Kållberg, P., Köhler, M., Matricardi, M., McNally, A. P., Monge-Sanz, B. M., Morcrette, J. J., Park, B. K., Peubey, C., de Rosnay, P., Tavolato, C., Thépaut, J. N., and Vitart, F.: The ERA-Interim reanalysis: configuration and performance of the data assimilation system, Q. J. Roy. Meteor. Soc., 137, 553–597, 2011.

Dentener, F., Kinne, S., Bond, T., Boucher, O., Cofala, J., Generoso, S., Ginoux, P., Gong, S., Hoelzemann, J. J., Ito, A., Marelli, L., Penner, J. E., Putaud, J.-P., Textor, C., Schulz, M., van der Werf, G. R., and Wilson, J.: Emissions of primary aerosol and precursor gases in

the years 2000 and 1750 prescribed data-sets for AeroCom, Atmos. Chem. Phys., 6, 4321–4344, doi:10.5194/acp-6-4321-2006, 2006.

Dirksen, R. J., Folkert Boersma, K., de Laat, J., Stammes, P., van der Werf, G. R., Val Martin, M., and Kelder, H. M.: An aerosol boomerang: rapid around-the-world transport of smoke from the December 2006 Australian forest fires observed from space, J. Geophys. Res.-Atmos., 114, D21201, doi:10.1029/2009JD012360, 2009.

Edwards, D. P., Emmons, L. K., Gille, J. C., Chu, A., Attié, J. L., Giglio, L., Wood, S. W., Haywood, J., Deeter, M. N., Massie, S. T., Ziskin, D. C., and Drummond, J. R.: Satellite-observed pollution from Southern Hemisphere biomass burning, J. Geophys. Res.-Atmos., 111, D14312, doi:10.1029/2005JD006655, 2006.

Field, R. D., van der Werf, G. R., and Shen, S. S. P.: Human amplification of drought-induced biomass burning in Indonesia since 1960, Nat. Geosci., 2, 185–188, 2009.

Fountoukis, C. and Nenes, A.: ISORROPIA II: a computationally efficient thermodynamic equilibrium model for K^+–Ca^{2+}–Mg^{2+}–NH_4^+–Na^+–SO_4^{2-}–NO_3^-–Cl^-–H_2O aerosols, Atmos. Chem. Phys., 7, 4639–4659, doi:10.5194/acp-7-4639-2007, 2007.

Fromm, M., Alfred, J., Hoppel, K., Hornstein, J., Bevilacqua, R., Shettle, E., Servranckx, R., Li, Z., and Stocks, B.: Observations of boreal forest fire smoke in the stratosphere by POAM III, SAGE II, and lidar in 1998, Geophys. Res. Lett., 27, 1407–1410, 2000.

Galanter, M., Levy, H., and Carmichael, G. R.: Impacts of biomass burning on tropospheric CO, NO_x, and O_3, J. Geophys. Res.-Atmos., 105, 6633–6653, 2000.

Granier, C., Bessagnet, B., Bond, T., D'Angiola, A., Denier van der Gon, H., Frost, G., Heil, A., Kaiser, J., Kinne, S., Klimont, Z., Kloster, S., Lamarque, J.-F., Liousse, C., Masui, T., Meleux, F., Mieville, A., Ohara, T., Raut, J.-C., Riahi, K., Schultz, M., Smith, S., Thompson, A., van Aardenne, J., van der Werf, G., and van Vuuren, D.: Evolution of anthropogenic and biomass burning emissions of air pollutants at global and regional scales during the 1980–2010 period, Climatic Change, 109, 163–190, 2011.

Guan, H., Chatfield, R. B., Freitas, S. R., Bergstrom, R. W., and Longo, K. M.: Modeling the effect of plume-rise on the transport of carbon monoxide over Africa with NCAR CAM, Atmos. Chem. Phys., 8, 6801–6812, doi:10.5194/acp-8-6801-2008, 2008.

Guenther, A. B., Jiang, X., Heald, C. L., Sakulyanontvittaya, T., Duhl, T., Emmons, L. K., and Wang, X.: The Model of Emissions of Gases and Aerosols from Nature version 2.1 (MEGAN2.1): an extended and updated framework for modeling biogenic emissions, Geosci. Model Dev., 5, 1471–1492, doi:10.5194/gmd-5-1471-2012, 2012.

Sensitivity of tropospheric loads and lifetimes of short lived pollutants

N. Daskalakis et al.

Title Page

Abstract | Introduction

Conclusions | References

Tables | Figures

◄ | ►

◄ | ►

Back | Close

Full Screen / Esc

Printer-friendly Version

Interactive Discussion

Hodzic, A., Vautard, R., Chepfer, H., Goloub, P., Menut, L., Chazette, P., Deuzé, J. L., Apituley, A., and Couvert, P.: Evolution of aerosol optical thickness over Europe during the August 2003 heat wave as seen from CHIMERE model simulations and POLDER data, Atmos. Chem. Phys., 6, 1853–1864, doi:10.5194/acp-6-1853-2006, 2006.

Honrath, R. E., Owen, R. C., Martin, M. V., Reid, J. S., Lapina, K., Fialho, P., Dziobak, M. P., Kleissl, J., and Westphal, D. L.: Regional and hemispheric impacts of anthropogenic and biomass burning emissions on summertime CO and O_3 in the North Atlantic lower free troposphere, J. Geophys. Res., 109, D24310, doi:10.1029/2004jd005147, 2004.

Jaffe, D., Bertschi, I., Jaeglé, L., Novelli, P., Reid, J. S., Tanimoto, H., Vingarzan, R., and Westphal, D. L.: Long-range transport of Siberian biomass burning emissions and impact on surface ozone in western North America, Geophys. Res. Lett., 31, L16106, doi:10.1029/2004GL020093, 2004.

Jian, Y. and Fu, T.-M.: Injection heights of springtime biomass-burning plumes over peninsular Southeast Asia and their impacts on long-range pollutant transport, Atmos. Chem. Phys., 14, 3977–3989, doi:10.5194/acp-14-3977-2014, 2014.

Kanakidou, M. and Crutzen, P. J.: The photochemical source of carbon monoxide: importance, uncertainties and feedbacks, Chemosphere, 1, 91–109, 1999.

Kanakidou, M., Duce, R. A., Prospero, J. M., Baker, A. R., Benitez-Nelson, C., Dentener, F. J., Hunter, K. A., Liss, P. S., Mahowald, N., Okin, G. S., Sarin, M., Tsigaridis, K., Uematsu, M., Zamora, L. M., and Zhu, T.: Atmospheric fluxes of organic N and P to the global ocean, Global Biogeochem. Cy., 26, GB3026, doi:10.10.1029/2011GB004277, 2012.

Keywood, M., Kanakidou, M., Stohl, A., Dentener, F., Grassi, G., Meyer, C. P., Torseth, K., Edwards, D., Thompson, A. M., Lohmann, U., and Burrows, J.: Fire in the air: biomass burning impacts in a changing climate, Crit. Rev. Env. Sci. Tec., 43, 40–83, 2013.

Klimont, Z., Smith, S. J., and Cofala, J.: The last decade of global anthropogenic sulfur dioxide: 2000–2011 emissions, Environ. Res. Lett., 8, 014003, doi:10.1088/1748-9326/8/1/014003, 2013.

Lavoué, D., Liousse, C., Cachier, H., Stocks, B. J., and Goldammer, J. G.: Modeling of carbonaceous particles emitted by boreal and temperate wildfires at northern latitudes, J. Geophys. Res.-Atmos., 105, 26871–26890, 2000.

Lelieveld, J., van Aardenne, J., Fischer, H., de Reus, M., Williams, J., and Winkler, P.: Increasing ozone over the Atlantic Ocean, Science, 304, 1483–1487, 2004.

Title Page

Abstract | Introduction

Conclusions | References

Tables | Figures

|◄ | ►|

◄ | ►

Back | Close

Full Screen / Esc

Printer-friendly Version

Interactive Discussion

Leung, F.-Y. T., Logan, J. A., Park, R., Hyer, E., Kasischke, E., Streets, D., and Yurganov, L.: Impacts of enhanced biomass burning in the boreal forests in 1998 on tropospheric chemistry and the sensitivity of model results to the injection height of emissions, J. Geophys. Res.-Atmos., 112, D10313, doi:10.1029/2006JD008132, 2007.

Levine, J. S., Cofer, W. R., Cahoon, D. R., and Winstead, E. L.: A driver for global change, Environ. Sci. Technol., 29, 120A–125A, 1995.

Mutch, R. W.: Fighting fire with prescribed fire: a return to ecosystem health, J. Forest., 92, 31–33, 1994.

Myriokefalitakis, S., Vignati, E., Tsigaridis, K., Papadimas, C., Sciare, J., Mihalopoulos, N., Facchini, M. C., Rinaldi, M., Dentener, F. J., Ceburnis, D., Hatzianastasiou, N., O'Dowd, C. D., van Weele, M., and Kanakidou, M.: Global modeling of the oceanic source of organic aerosols, Adv. Meteorol., 2010, 1–16, 2010.

Myriokefalitakis, S., Tsigaridis, K., Mihalopoulos, N., Sciare, J., Nenes, A., Kawamura, K., Segers, A., and Kanakidou, M.: In-cloud oxalate formation in the global troposphere: a 3-D modeling study, Atmos. Chem. Phys., 11, 5761–5782, doi:10.5194/acp-11-5761-2011, 2011.

Nenes, A., Pandis, S., and Pilinis, C.: ISORROPIA: a new thermodynamic equilibrium model for multiphase multicomponent inorganic aerosols, Aquat. Geochem., 4, 123–152, 1998.

Pfister, G., Hess, P. G., Emmons, L. K., Lamarque, J. F., Wiedinmyer, C., Edwards, D. P., Pétron, G., Gille, J. C., and Sachse, G. W.: Quantifying CO emissions from the 2004 Alaskan wildfires using MOPITT CO data, Geophys. Res. Lett., 32, L11809, doi:10.1029/2005GL022995, 2005.

Reid, J. S., Eck, T. F., Christopher, S. A., Koppmann, R., Dubovik, O., Eleuterio, D. P., Holben, B. N., Reid, E. A., and Zhang, J.: A review of biomass burning emissions part III: intensive optical properties of biomass burning particles, Atmos. Chem. Phys., 5, 827–849, doi:10.5194/acp-5-827-2005, 2005.

Rosenfeld, D.: TRMM observed first direct evidence of smoke from forest fires inhibiting rainfall, Geophys. Res. Lett., 26, 3105–3108, 1999.

Simmonds, P. G., Manning, A. J., Derwent, R. G., Ciais, P., Ramonet, M., Kazan, V., and Ryall, D.: A burning question. Can recent growth rate anomalies in the greenhouse gases be attributed to large-scale biomass burning events?, Atmos. Environ., 39, 2513–2517, 2005.

Sofiev, M., Ermakova, T., and Vankevich, R.: Evaluation of the smoke-injection height from wildland fires using remote-sensing data, Atmos. Chem. Phys., 12, 1995–2006, doi:10.5194/acp-12-1995-2012, 2012.

Title Page

Abstract | Introduction

Conclusions | References

Tables | Figures

◄ | ►

◄ | ►

Back | Close

Full Screen / Esc

Printer-friendly Version

Interactive Discussion

Sofiev, M., Vankevich, R., Ermakova, T., and Hakkarainen, J.: Global mapping of maximum emission heights and resulting vertical profiles of wildfire emissions, Atmos. Chem. Phys., 13, 7039–7052, doi:10.5194/acp-13-7039-2013, 2013.

Tsigaridis, K. and Kanakidou, M.: Global modelling of secondary organic aerosol in the troposphere: a sensitivity analysis, Atmos. Chem. Phys., 3, 1849–1869, doi:10.5194/acp-3-1849-2003, 2003.

Tsigaridis, K. and Kanakidou, M.: Secondary organic aerosol importance in the future atmosphere, Atmos. Environ., 41, 4682–4692, 2007.

Tsigaridis, K., Daskalakis, N., Kanakidou, M., Adams, P. J., Artaxo, P., Bahadur, R., Balkanski, Y., Bauer, S. E., Bellouin, N., Benedetti, A., Bergman, T., Berntsen, T. K., Beukes, J. P., Bian, H., Carslaw, K. S., Chin, M., Curci, G., Diehl, T., Easter, R. C., Ghan, S. J., Gong, S. L., Hodzic, A., Hoyle, C. R., Iversen, T., Jathar, S., Jimenez, J. L., Kaiser, J. W., Kirkevåg, A., Koch, D., Kokkola, H., Lee, Y. H., Lin, G., Liu, X., Luo, G., Ma, X., Mann, G. W., Mihalopoulos, N., Morcrette, J.-J., Müller, J.-F., Myhre, G., Myriokefalitakis, S., Ng, S., O'Donnell, D., Penner, J. E., Pozzoli, L., Pringle, K. J., Russell, L. M., Schulz, M., Sciare, J., Seland, Ø., Shindell, D. T., Sillman, S., Skeie, R. B., Spracklen, D., Stavrakou, T., Steenrod, S. D., Takemura, T., Tiitta, P., Tilmes, S., Tost, H., van Noije, T., van Zyl, P. G., von Salzen, K., Yu, F., Wang, Z., Wang, Z., Zaveri, R. A., Zhang, H., Zhang, K., Zhang, Q., and Zhang, X.: The AeroCom evaluation and intercomparison of organic aerosol in global models, Atmos. Chem. Phys. Discuss., 14, 6027–6161, doi:10.5194/acpd-14-6027-2014, 2014.

Val Martin, M., Logan, J. A., Kahn, R. A., Leung, F.-Y., Nelson, D. L., and Diner, D. J.: Smoke injection heights from fires in North America: analysis of 5 years of satellite observations, Atmos. Chem. Phys., 10, 1491–1510, doi:10.5194/acp-10-1491-2010, 2010.

Val Martin, M., Kahn, R. A., Logan, J. A., Paugam, R., Wooster, M., and Ichoku, C.: Space-based observational constraints for 1-D fire smoke plume-rise models, J. Geophys. Res.-Atmos., 117, doi:10.1029/2012JD018370, 2012.

van der Werf, G. R., Randerson, J. T., Giglio, L., Collatz, G. J., Kasibhatla, P. S., and Arellano Jr., A. F.: Interannual variability in global biomass burning emissions from 1997 to 2004, Atmos. Chem. Phys., 6, 3423–3441, doi:10.5194/acp-6-3423-2006, 2006.

van der Werf, G. R., Randerson, J. T., Giglio, L., Collatz, G. J., Mu, M., Kasibhatla, P. S., Morton, D. C., DeFries, R. S., Jin, Y., and van Leeuwen, T. T.: Global fire emissions and the contribution of deforestation, savanna, forest, agricultural, and peat fires (1997–2009), Atmos. Chem. Phys., 10, 11707–11735, doi:10.5194/acp-10-11707-2010, 2010.

Title Page

Abstract | Introduction

Conclusions | References

Tables | Figures

|◄ | ►|

◄ | ►

Back | Close

Full Screen / Esc

Printer-friendly Version

Interactive Discussion

Vignati, E., Facchini, M. C., Rinaldi, M., Scannell, C., Ceburnis, D., Sciare, J., Kanakidou, M., Myriokefalitakis, S., Dentener, F., and O'Dowd, C. D.: Global scale emission and distribution of sea-spray aerosol: sea-salt and organic enrichment, Atmos. Environ., 44, 670–677, 2010.

Wiedinmyer, C., Akagi, S. K., Yokelson, R. J., Emmons, L. K., Al-Saadi, J. A., Orlando, J. J., and Soja, A. J.: The Fire INventory from NCAR (FINN): a high resolution global model to estimate the emissions from open burning, Geosci. Model Dev., 4, 625–641, doi:10.5194/gmd-4-625-2011, 2011.

Williams, J. E., van Weele, M., van Velthoven, P. F. J., Scheele, M. P., Liousse, C., and van der Werf, G. R.: The impact of uncertainties in african biomass burning emission estimates on modeling global air quality, long range transport and tropospheric chemical lifetimes, Atmosphere, 3, 132–163, 2012.

Table 1. Anthropogenic emissions ($Tg\,a^{-1}$) used in this study and fraction of emissions that corresponds to the AWB sector included in the ECLIPSE anthropogenic emissions inventory. Both absolute quantities and percentage of the total anthropogenic emissions from (Klimont et al., 2013) are presented.

	BC	CO	NO$_x$	OC	SO$_x$	NMVOC
ECLPSE (with AWB)	5.38	527.1	43.97	11.56	45.95	140.47
AWB on ECLIPSE	0.33	27.46	0.14	1.28	0.09	5.20
% contribution of AWB to total anthropogenic	6.2	5.21	0.31	11.08	0.19	3.7

Full Screen / Esc

Printer-friendly Version

Interactive Discussion

Table 2. Total annual amounts of pollutants emitted by wild fires according to the different inventories used, for 2008 in $Tg\,a^{-1}$. NO_x is reported as NO.

	BC	CO	NO_x	OC	SO_2	NMVOC	NH_3
GFEDv3-ECLIPSE	1.695	264.205	3.751	15.197	0.940	15.552	3.320
GFEDv3	1.759	276.774	3.894	15.694	0.967	45.710	5.999
FINN	0.327	331.322	5.917	3.548	1.138	56.857	4.361
ACCMIP	2.620	460.419	5.479	23.309	1.929	80.869	9.203

Table 3. Wildfire emissions from the GFEDv3 inventory in $Tg\,a^{-1}$ and the AWB fraction in % contained in the inventory, for 2008. NO_x is reported as NO.

	BC	CO	NO_x	OC	SO_x	NMVOC
GFEDv3	1.76	276.77	3.89	15.69	0.97	45.71
AWB in GFEDv3	0.06	12.57	0.14	0.5	0.03	30.16
% contribution of AWB to total anthropogenic	3.66	4.54	3.67	3.16	2.78	65.98

Table 4. Summary of simulations performed for this work.

Height	GFEDv3-ECLIPSE Varying	GFEDv3-ECLIPSE Surface	GFEDv3 Varying	GFEDv3 Surface	ACCMIP Varying	ACCMIP Surface	FINN Varying	FINN Surface
S0.0	×							
S0.1		×						
S1.0			×					
S1.1				×				
S2.0					×			
S2.1						×		
S3.0							×	
S3.1								×
S4.0								

Table 5. Total annual mean tropospheric load of pollutants for all simulations in $Tg\,a^{-1}$.

	S0.0	S0.1	S1.0	S1.1	S2.0	S2.1	S3.0	S3.1	S4.0
CO	292.93	292.33	294.13	293.13	316.02	314.31	301.62	300.54	262.60
Ozone	299.59	298.98	299.75	299.23	305.35	304.53	305.53	304.50	290.49
NO_x	0.125	0.125	0.125	0.125	0.127	0.127	0.127	0.127	0.121
SO_4^{2-}	1.870	1.864	1.870	1.864	1.890	1.880	1.868	1.861	1.826
HNO_3	1.905	1.896	1.887	1.885	1.938	1.930	1.931	1.917	1.753
NH_4^+	0.488	0.476	0.503	0.458	0.505	0.485	0.490	0.477	0.450
Isoprene	0.264	0.265	0.264	0.265	0.245	0.246	0.252	0.253	0.312
OC	0.107	0.107	0.107	0.106	0.118	0.117	0.079	0.079	0.070
BC	0.133	0.133	0.129	0.129	0.143	0.143	0.092	0.092	0.086

Table 6. Calculated annual mean tropospheric lifetimes of pollutants for all the simulations performed.

	S0.0	S0.1	S1.0	S1.1	S2.0	S2.1	S3.0	S3.1	S4.0
CO (days)	39.91	39.88	40.02	39.93	40.33	40.18	39.75	39.71	40.26
Ozone (days)	18.01	18.03	17.98	18.00	17.87	17.90	17.86	17.89	18.31
NO_x (days)	0.714	0.712	0.718	0.715	0.712	0.709	0.708	0.704	0.731
NO_y (days)	6.546	6.509	6.571	6.533	6.631	6.572	6.817	6.733	6.430
SO_4^{2-} (days)	4.409	4.405	4.410	4.406	4.389	4.386	4.389	4.386	4.387
HNO_3 (days)	2.490	2.489	2.479	2.483	2.481	2.482	2.462	2.460	2.439
NH_4^+ (days)	4.949	4.900	4.999	4.929	4.931	4.873	4.897	4.860	4.827
Isoprene (hours)	4.451	4.468	4.457	4.473	4.127	4.142	4.246	4.261	5.262
OC (days)	6.036	6.003	6.053	6.017	5.932	5.901	5.401	5.393	5.294
BC (days)	6.966	6.947	6.998	6.977	6.928	6.910	6.332	6.331	6.290
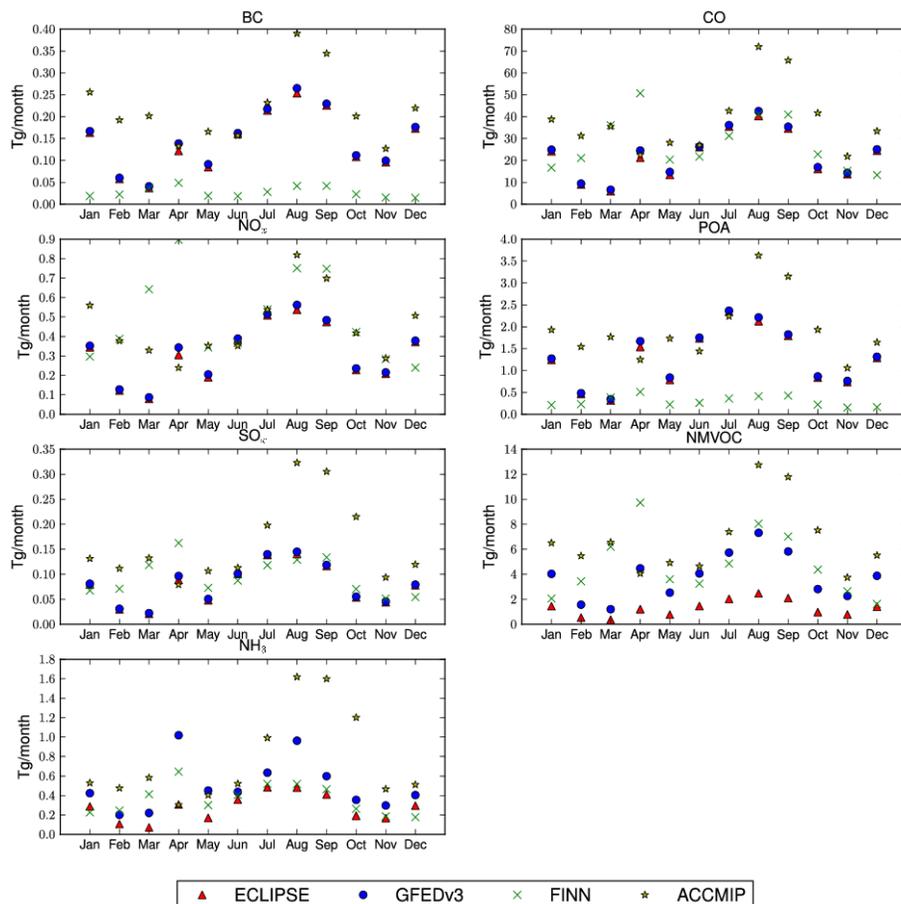
Figure 1. Monthly variation and differences of biomass burning emission inventories for the year 2008 for all species used in the model. For simplicity, NMVOC are summed up.
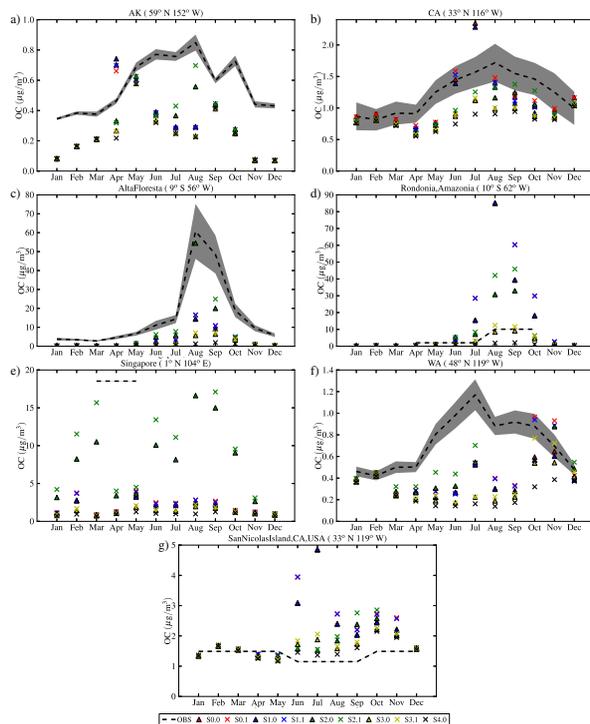
Figure 2. Comparison of monthly mean model results with observations of organic carbon (OC) at southern Alaska **(a)**, California State, USA **(b)**, Alta Floresta, Brazil **(c)**, Rondonia, Amazonia **(d)**, Singapore **(e)**, Washington State, USA **(f)** and San Nicolas Island, California, USA **(g)**. The dashed line with the gray shaded area shows the monthly mean value of observations with the standard deviation based on their interannual variability, while the colored symbols show the calculated values for the specific station. Triangles are for simulations assuming a vertical distribution of wildfire emissions, while the × symbols show the simulations assuming that all open biomass burning emissions occur near the surface. Details on the simulations are given in Table 4.

Title Page

Abstract | Introduction

Conclusions | References

Tables | Figures

|◄ | ►|

◄ | ►

Back | Close

Full Screen / Esc

Printer-friendly Version

Interactive Discussion

Full Screen / Esc

Printer-friendly Version

Interactive Discussion
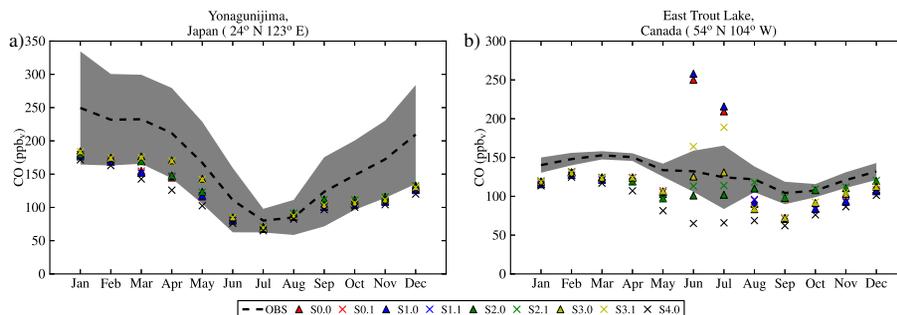
Figure 3. Comparison of monthly mean model results with CO surface observations at Yona-gunijima, Japan **(a)** and at East Trout Lake, Canada **(b)**. Lines and symbols as in Fig. 2 but for CO.
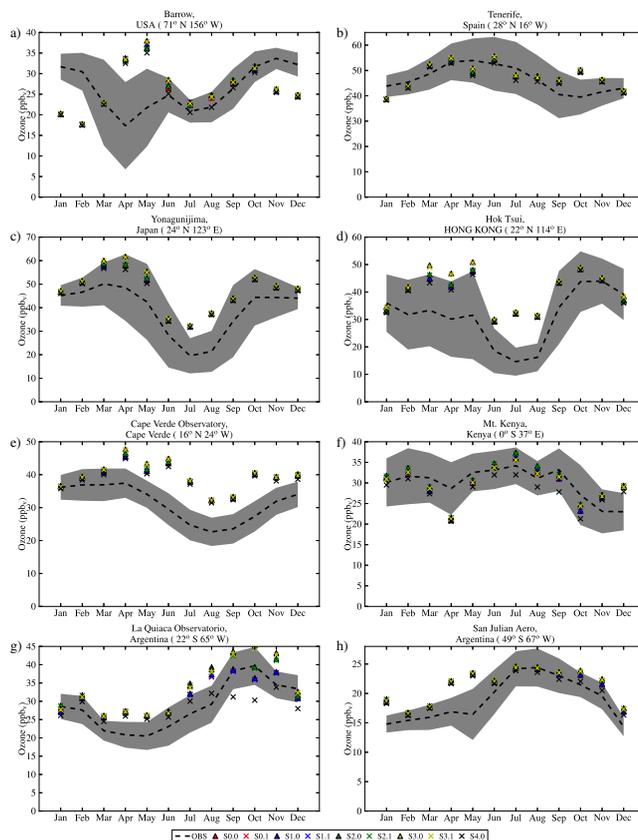
Figure 4. Comparison of monthly mean surface ozone measurements with model results at Barrow, USA **(a)**, Tenerife, Spain **(b)**, Yonagunijima, Japan **(c)**, Hok Tsui, Hong Kong **(d)**, Cape Verde Observatory, Cape Verde **(e)**, Mount Kenya, Kenya **(f)**, La Quiaca Observatory, Argentina **(g)** and San Julian Aero, Argentina **(h)**. Lines and symbols as in Fig. 2 but for O$_3$.

Title Page

Abstract | Introduction

Conclusions | References

Tables | Figures

|◀ | ▶|

◀ | ▶

Back | Close

Full Screen / Esc

Printer-friendly Version

Interactive Discussion
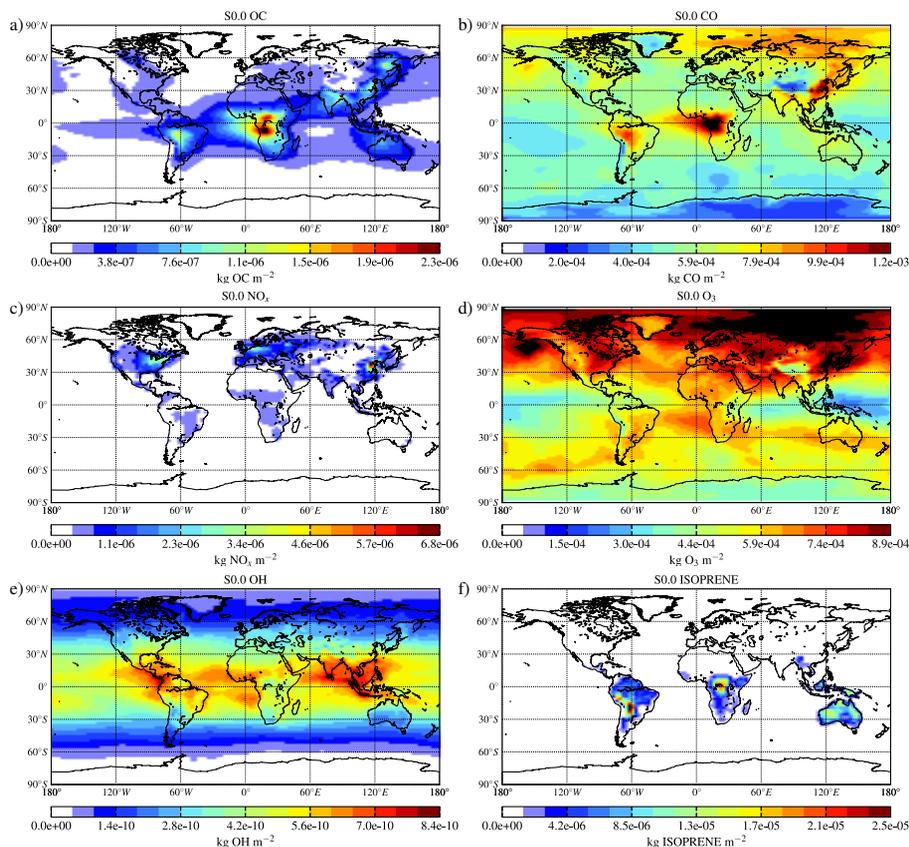
Figure 5. Calculated annual mean tropospheric load in (kg m^{-2}) of selected species for the base case scenario (S0.0). Areas with black exceed the maximum value of the colorbar.

Title Page

Abstract | Introduction

Conclusions | References

Tables | Figures

|◄ | ►|

◄ | ►

Back | Close

Full Screen / Esc

Printer-friendly Version

Interactive Discussion
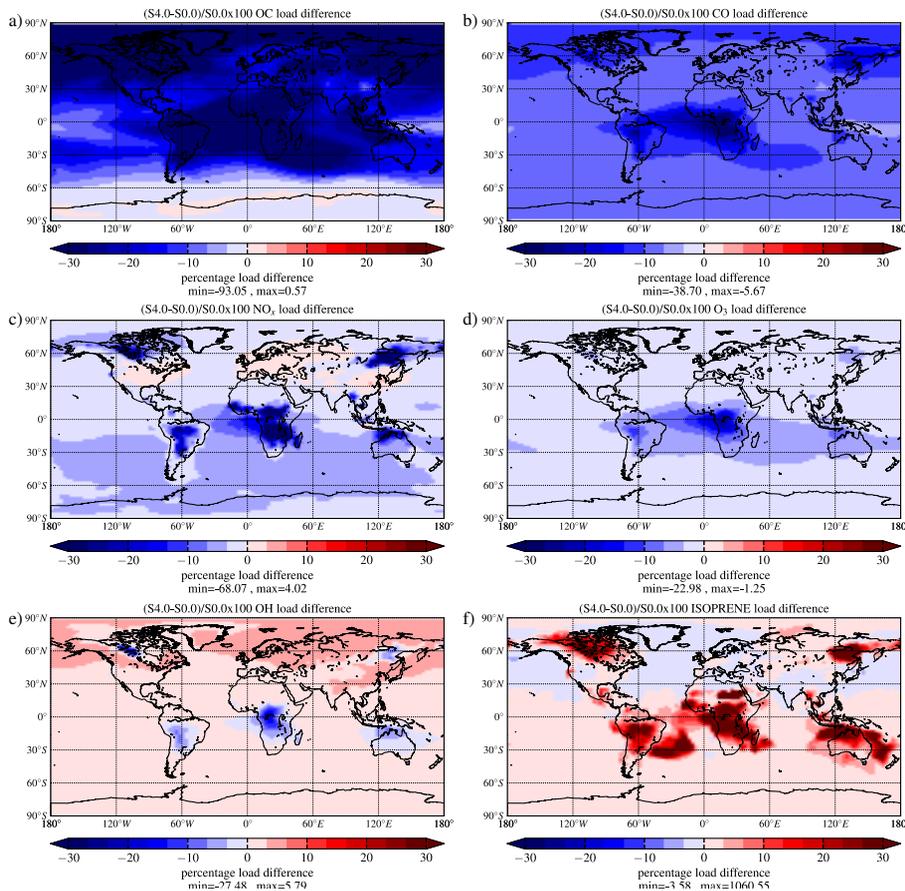
Figure 6. Percentage difference in the computed annual mean loads of OC **(a)**, CO **(b)**, NO_x **(c)**, O_3 **(d)**, OH **(e)**, isoprene **(f)** – attributed to wildfire emissions calculated as (column_S4.0 – column_S0.0)/(column S0.0) × 100. The scale is from −30 % to 30 % ; the minimum and maximum differences are printed under each panel.

Title Page

Abstract · Introduction

Conclusions · References

Tables · Figures

|◄ · ►|

◄ · ►

Back · Close

Full Screen / Esc

Printer-friendly Version

Interactive Discussion
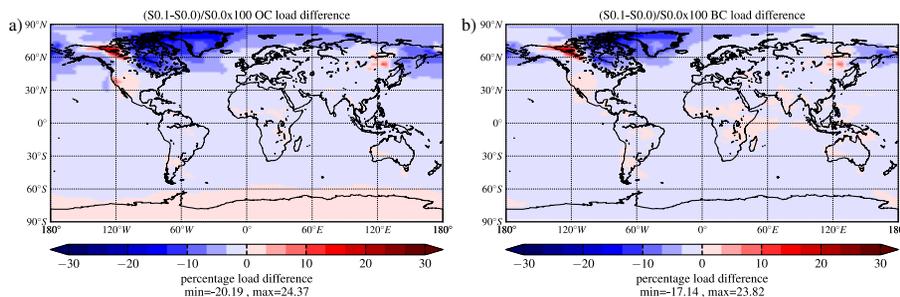
Figure 7. Percentage difference of annual mean computed tropospheric load of OC **(a)** and BC **(b)** attributed to wildfire emission injection height calculated as (load_S0.1 – load_S0.0)/(load S0.0) × 100. The scale is from −30 % to 30 %; the minimum and maximum differences are printed under each panel.
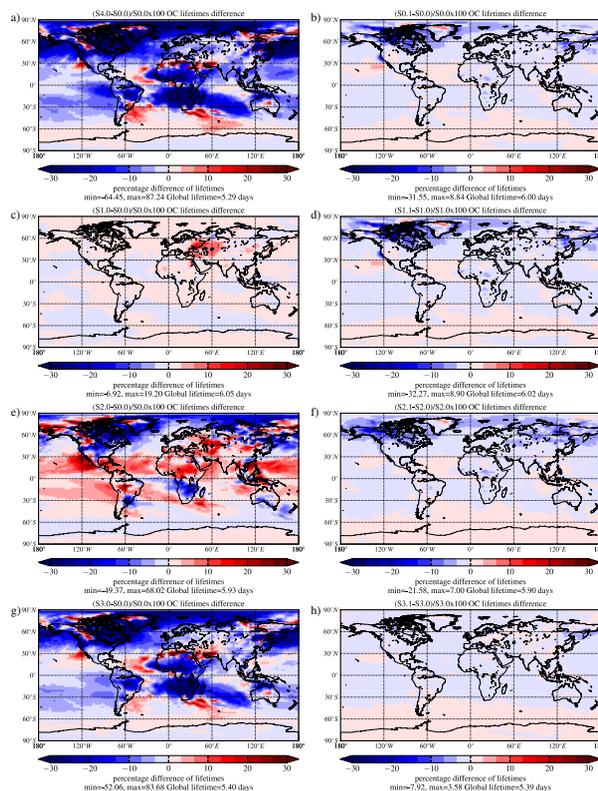
Figure 8. Percent impact on the computed annual mean tropospheric lifetime of OC of: (left panels) the different emission inventories calculated as the percent difference between simulations SX.0 and simulation S0.0; and of (right panels) height distribution calculated as the percent difference between simulations SX.1 and simulations SX.0 The colorbar ranges from −30 % to 30 %. The minimum and maximum local lifetimes as well as the global lifetime are printed under each panel.
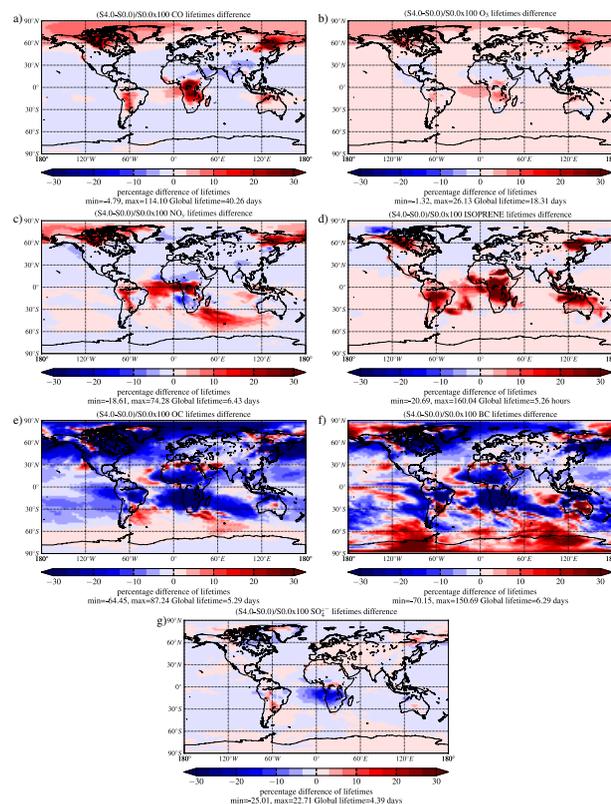
Figure 9. Percent impact of wild fire emissions to the computed annual mean lifetimes of CO **(a)**, O_3 **(b)**, NO_y **(c)**, isoprene **(d)**, OC **(e)**, BC **(f)** and SO_4^{2-} **(g)** depicted as the percentage difference of S4.0 and S0.0. The colorbar ranges from -30% to 30%. The minimum and maximum local lifetimes as well as the global lifetime are printed under each panel.
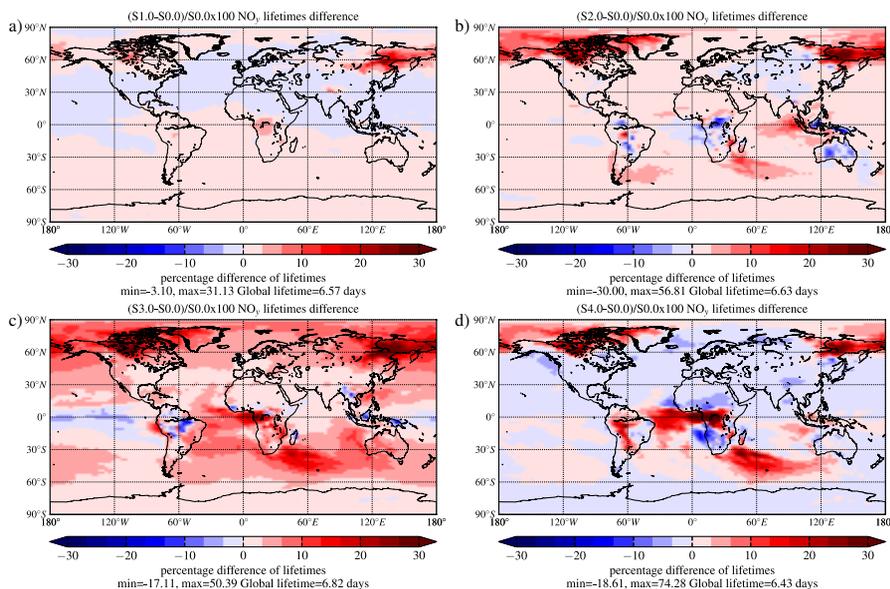
Figure 10. Computed annual mean tropospheric NO$_y$ lifetimes differences between the base case scenario (S0.0) and S1.0 **(a)**, S2.0 **(b)**, S3.0 **(c)** and S4.0 **(d)**, computed by reference to S0.0. The colorbar ranges from −30 % to 30 %. The minimum and maximum local lifetimes as well as the global lifetime are printed under each panel.

Discussion Paper | Discussion Paper | Discussion Paper | Discussion Paper |

ACPD

14, 22639–22676, 2014

Sensitivity of tropospheric loads and lifetimes of short lived pollutants

N. Daskalakis et al.

Title Page

Abstract | Introduction

Conclusions | References

Tables | Figures

|◄ | ►|

◄ | ►

Back | Close

Full Screen / Esc

Printer-friendly Version

Interactive Discussion